A 3D engineered tumour for spatial snap-shot analysis of cell metabolism and phenotype in hypoxic gradients.

Darren Rodenhizer[1], Edoardo Gaude[2], Dan Cojocari[3], Radhakrishnan Mahadevan[1,4], Christian Frezza[2], Bradly G. Wouters[3], Alison P. McGuigan[1,4 *]

[1] University of Toronto, Department of Chemical Engineering and Applied Chemistry 200 College St. Toronto, ON M5S 3E5, Canada, Phone: 416 978 7552

[2] MRC Cancer Unit, University of Cambridge, Hutchison/MRC Research Centre, Box 197, Cambridge Biomedical Campus, Cambridge, CB2 0XZ, United Kingdom

[3] Princess Margaret Cancer Centre and Campbell Family Institute for Cancer Research, Departments of Medical Biophysics and Radiation Oncology, University Health Network, Toronto, ON M5G 2M9, Canada

[4] Institute of Biomaterials and Biomedical Engineering, University of Toronto

** To whom correspondence show be addressed (Alison.mcguigan@utoronto.ca)*

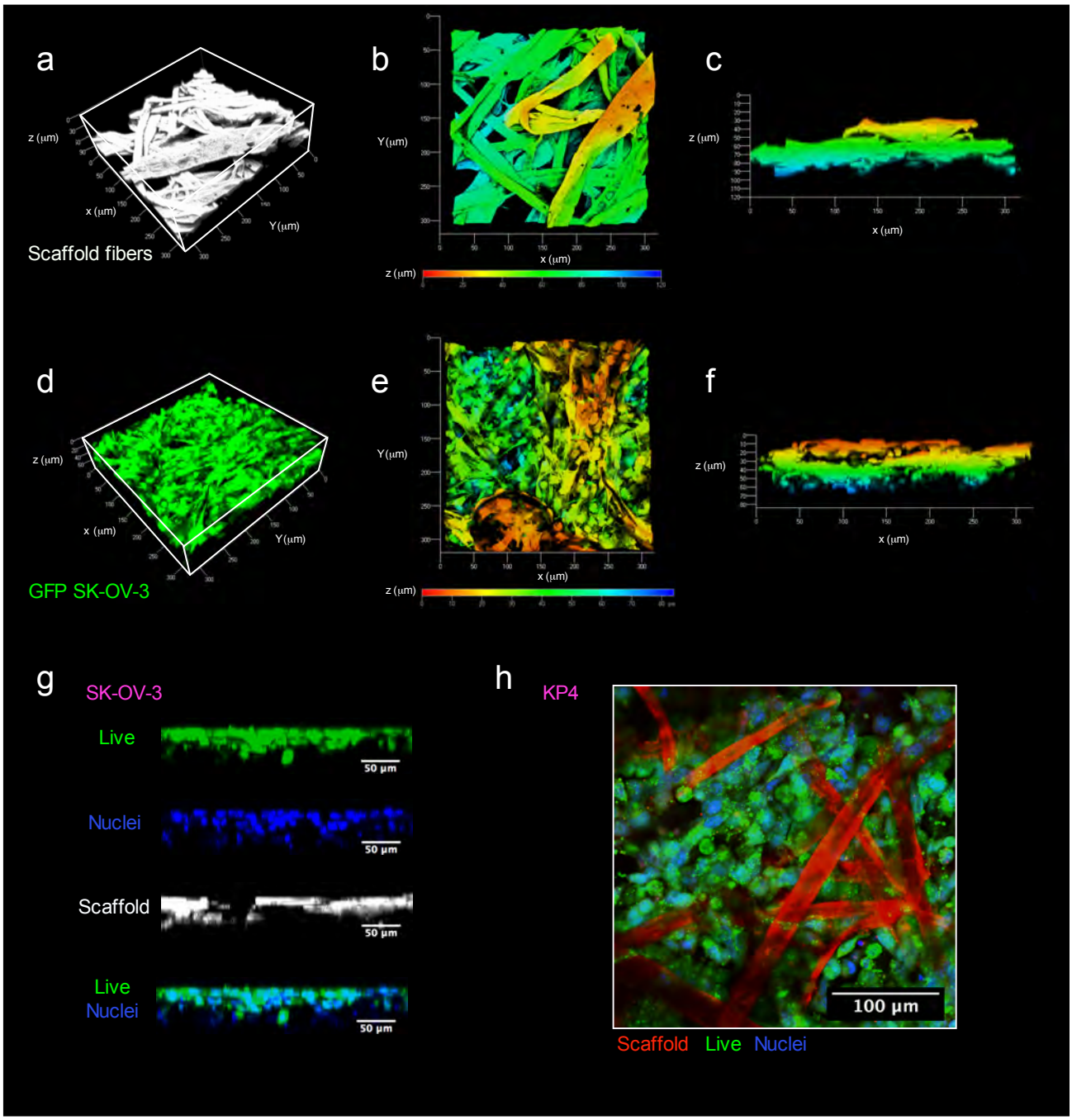

Supplementary figure 1: Confocal depth profiling of scaffold and a single biocomposite layer. a-c – 3D confocal reconstruction of the cellulose scaffold showing interlocking of fibers (a) and color coded to map the depth of fibers within the scaffold relative to the top of the z-stack, in a top down view (b) and side profile (c). Detailed fiber imaging was achieved by labelling the scaffold with fluorescein. d-f – 3D confocal reconstruction of a separate biocomposite sample shows the thick and 3D nature of SK-OV-3 cells expressing GFP within the scaffold (d) and color coded to indicate the depth of individual cells relative to the top of the z stack in a top down view (e) and side view (f). After remodelling the thickness of the biocomposite strip was 34.19 µm ±4.38 µm (mean± SEM for n=18). g – side profile projections (50µm of thickness) showing 3D structure of biocomposite and indicating live cells (green – calcein AM), nuclei (blue – DRAQ5) and the scaffold (autofluorescence), and combined. h – Interlocking of cells and scaffold fibers is demonstrated in this 2µm thick confocal section of a biocomposite containing live KP4 cells (green-calcein AM), nuclei (blue – DRAQ5) and scaffold fibers (red – autofluorescence).

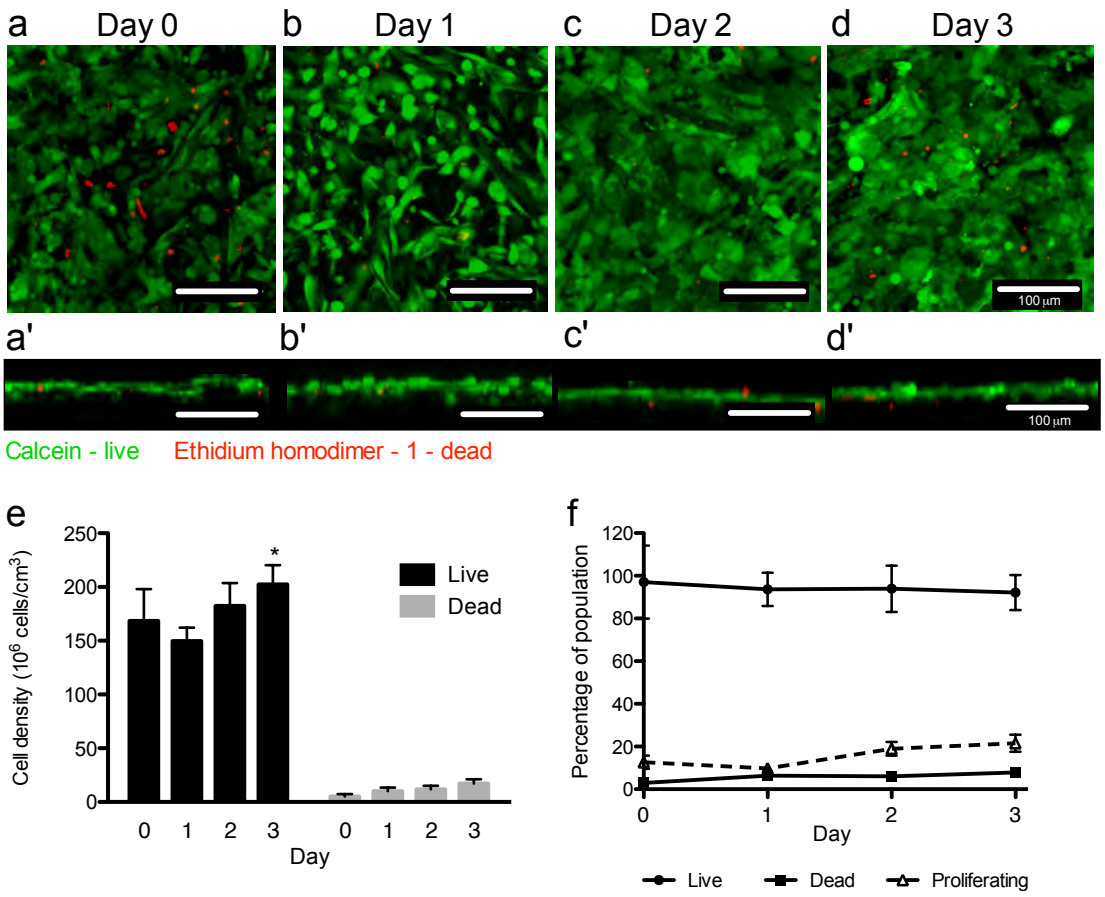

Supplementary figure 2: Cell viability and growth in single biocomposite layer. a-d - Live (green – calcein AM) and dead (red – ethidium homodimer 1) stained cells in a single non-rolled biocomposite layer after (a) 0, (b) 1, (c) 2, or (d) 3 days of culture. Images a'-d' show side profile reconstructions of the layer (50µm thickness). e- Live and dead cell density in the biocomposite as a function of time. Live cells numbers at day 3 are significantly different than day 1 ($p \leq 0.05$). f – Percentage of live, dead and proliferating cells in the non-rolled construct over time. Graphs e and f were produced from quantitative analysis of confocal images stained for nuclei (DRAQ5), dead cells (ethidium homodimer-1) and proliferating cells (KI67 positive). Error bars are SEM for n = 9 measurements from 3 samples.

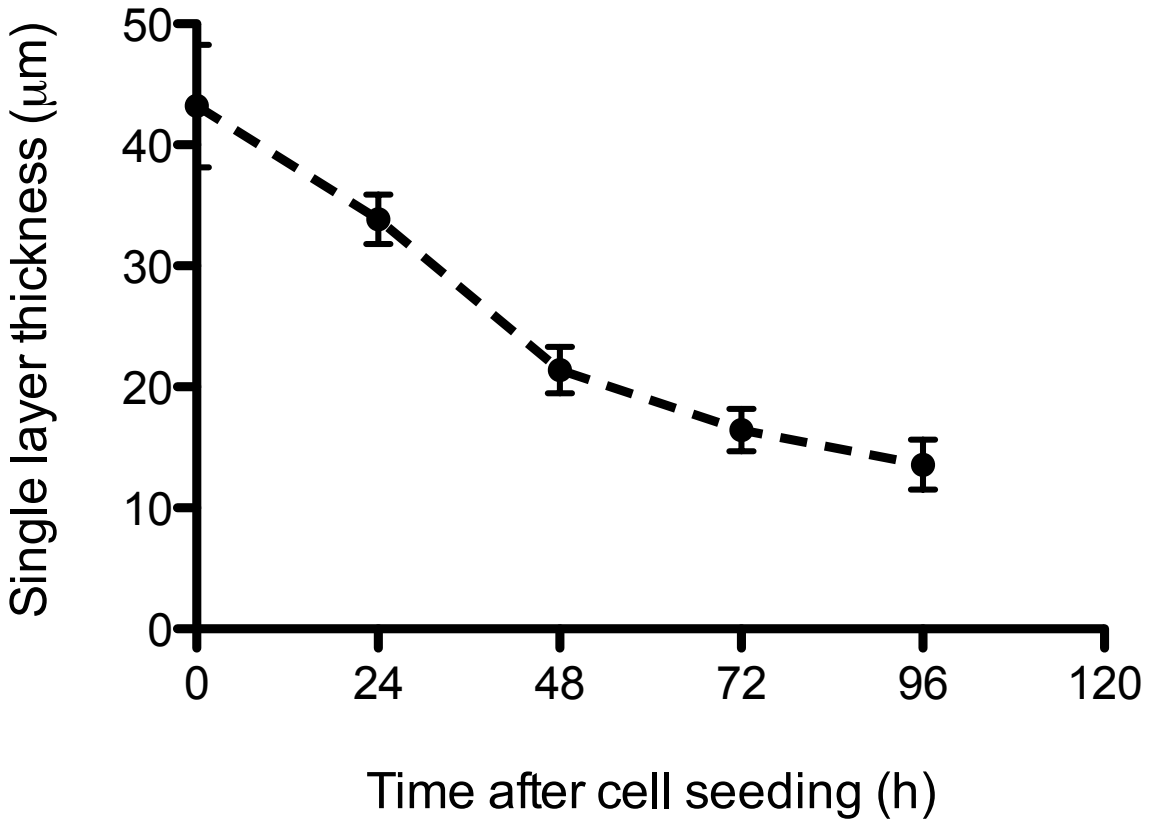

Supplementary figure 3: Single layer thickness as a function of time. To assess cell remodelling in the biocomposite, single layers were cultured for 0, 1, 2, and 3 days followed by calcein AM staining to label live cells. Confocal Z-stacks were acquired from each sample and used to assess biocomposite thickness. Cell remodelling results in layer compaction, which plateaus after 2 days. It was observed that layer integrity is achieved after 24h, which allows handling, and rolling of the strip. Error bars are standard deviation (n = 3).

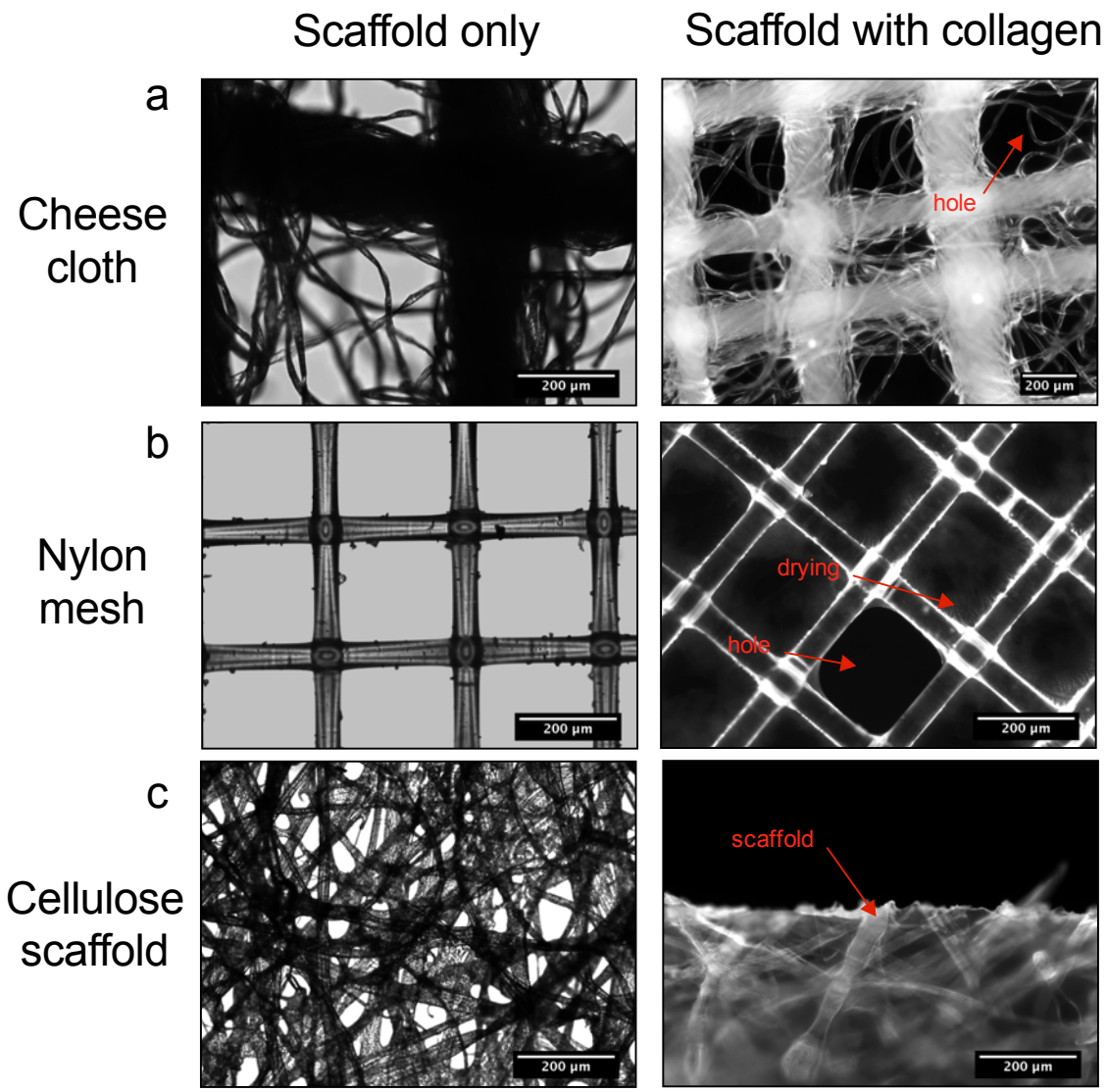

Supplementary figure 4: Scaffold Materials Selection. Scaffold selection was based on the ability to gel a thin layer of collagen of consistent thickness without excessive drying of the collagen, or formation of holes or voids. Fluorescein was added to the collagen to aid in visualization. Brightfield and fluorescence images of: a- #90 grade cheese cloth without and with collagen showing large variability in collagen sheet thickness due to large and varying pore sizes. b- Nylon mesh without and with collagen showing drying of the collagen and void formation. c- Cellulose scaffolding without and with collagen showing consistent collagen gelling and thickness without excessive drying.

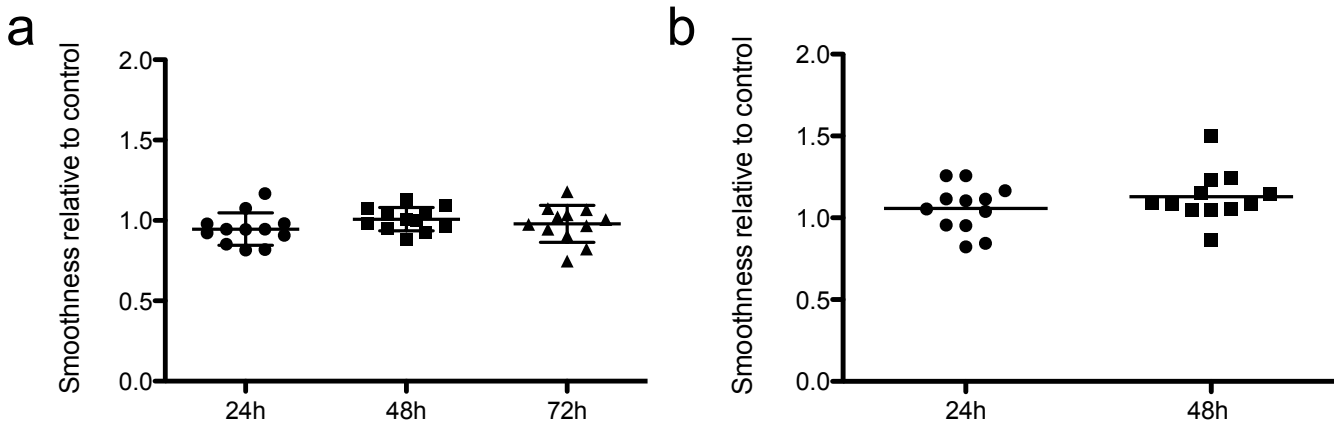

Supplementary figure 5: Scaffold integrity after unrolling. The smoothness of layer interfaces in the TRACER were assessed after unrolling to determine if the sectioning process resulted in layer destruction (identified by a decrease in smoothness compared to a non-rolled layer surface). a- smoothness measurements in TRACERs containing SK-OV-3 cells after 1, 2 and 3 days of rolled culture and b- KP4 cells after 1 and 2 days of rolled culture. Smoothness at each time point was not significantly different between any groups. Smoothness measurements were normalized to the appropriate interface of a layer that was never rolled, but was cultured for 24h. n = 12 measurements were made from 1 TRACER at each time point for both (a) and (b).

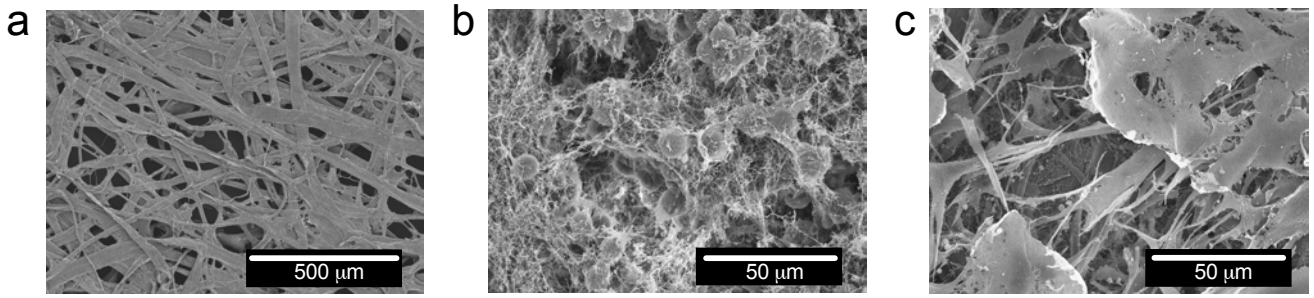

Supplementary figure 6: SEM characterization of a single layer biocomposite. a- SEM of cellulose scaffold before infiltration with collagen and cells. b – SEM of scaffold containing NIH 3T3 fibroblast cells and collagen immediately after cell seeding. Cells can be seen as rounded structures surrounded by collagen fibers. c – SEM of biocomposite after 24h of culture showing cells as flat, stretching structures with supporting collagen fibers.

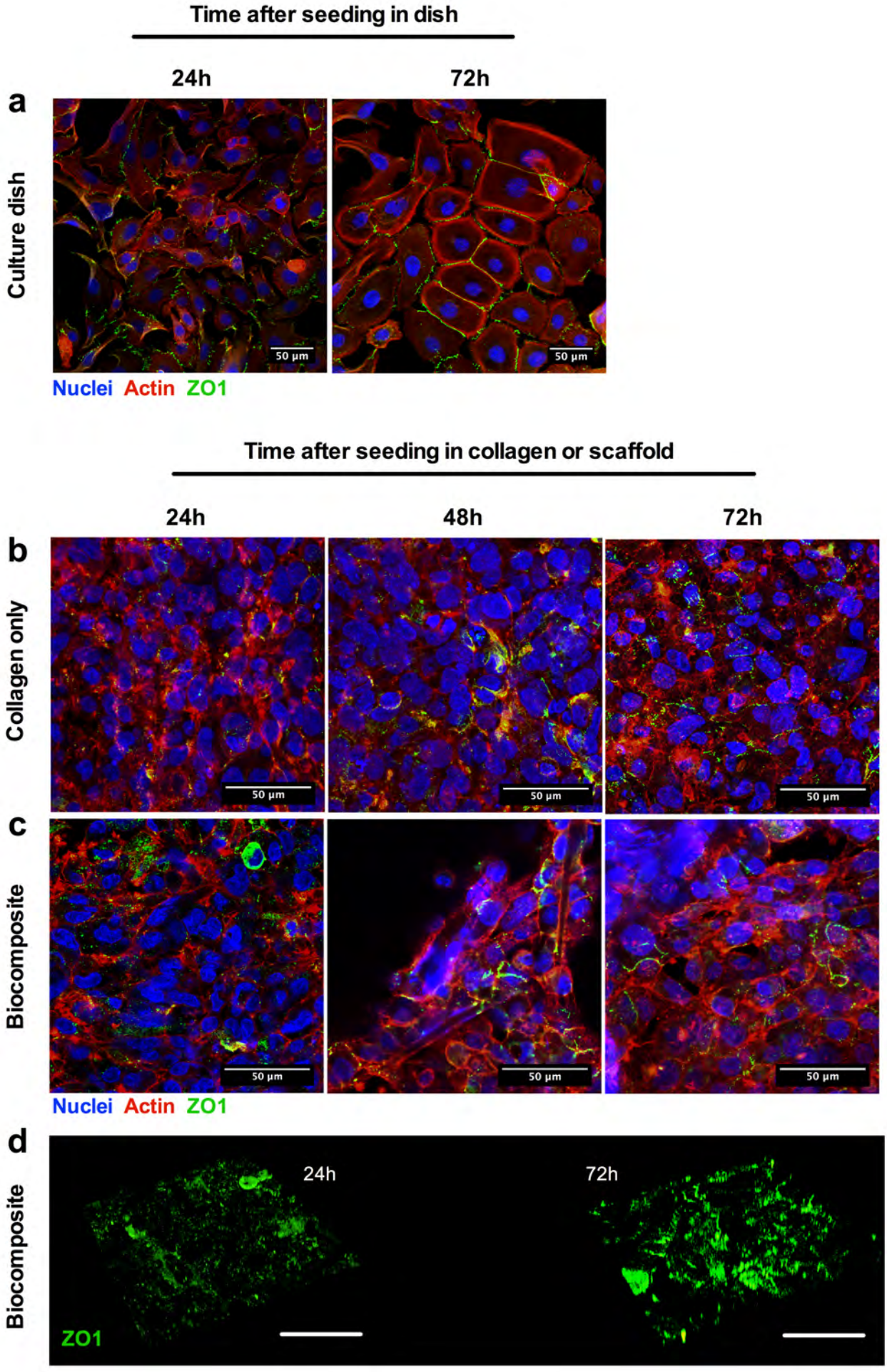
Time after seeding in dish
24h
72h
a
Culture dish
50 µm
50 µm
Nuclei Actin ZO1
Time after seeding in collagen or scaffold
24h
48h
72h
b
Collagen only
50 µm
50 µm
50 µm
c
Biocomposite
50 µm
50 µm
50 µm
Nuclei Actin ZO1
d
Biocomposite
24h
72h
ZO1

Supplementary Figure 7: Junction maturation of a single layer biocomposite. a – Thin (2µm) confocal optical sections showing the actin cytoskeleton of SK-OV-3 cells after 24, and 72h in a 2D culture dish. b-c - Thin (1-10µ m) z projections of SK-OV-3 cells in collagen only gel (b) or the biocomposite (c) after 24, 48, or 72h of culture . Actin fibres are labelled with phalloidin (red), ZO-1 (green) indicates the presence of cell-cell junctions, and nuclei are labelled with DRAQ5 (blue). Similar cell morphologies are observed in both (b) and (c) at each time point with junctions appearing most mature at 72h. d- 3D projections of ZO-1 junctions in the biocomposite at 24 and 72h**.**

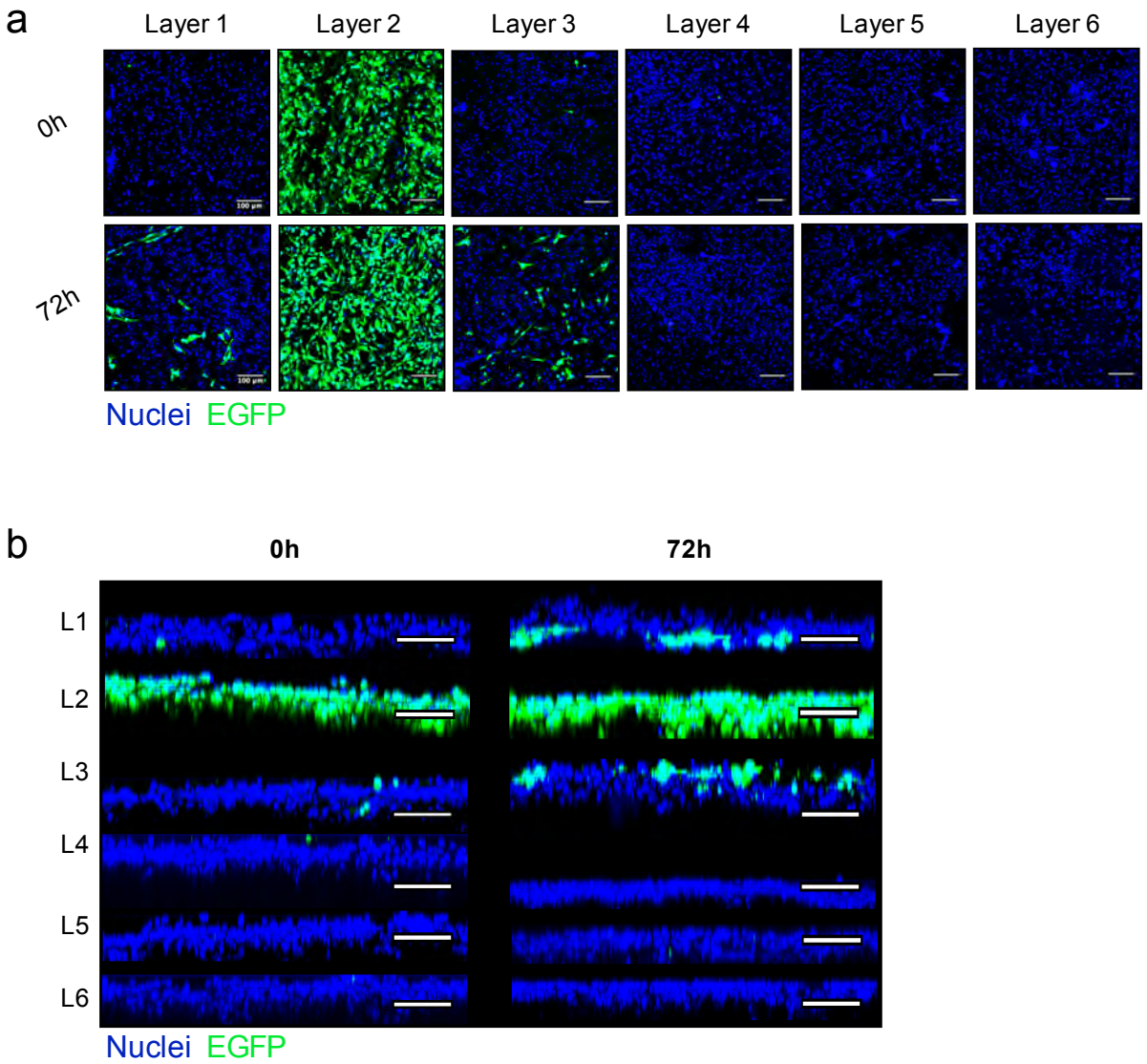

Supplementary Figure 8: Cell migration between adjacent TRACER layers. – To assess cell movement of SK-OV-3 cells between adjacent layers, TRACERS were fabricated with GFP positive cells in layer 2 and wild type cells in all other layers and cultured in the rolled configuration for 3 days. TRACERs were then unrolled and assessed with confocal microscopy for movement of the GFP cells to adjacent layers. a- confocal z-projections showing nuclei (DRAQ5 – blue) and GFP positive cells (green) in each layer of a TRACER before rolling and after 3 days of rolled culture. Minor GFP cell transfer can be seen on adjacent surfaces to layer 2. b- Images from (a) presented as side profiles.

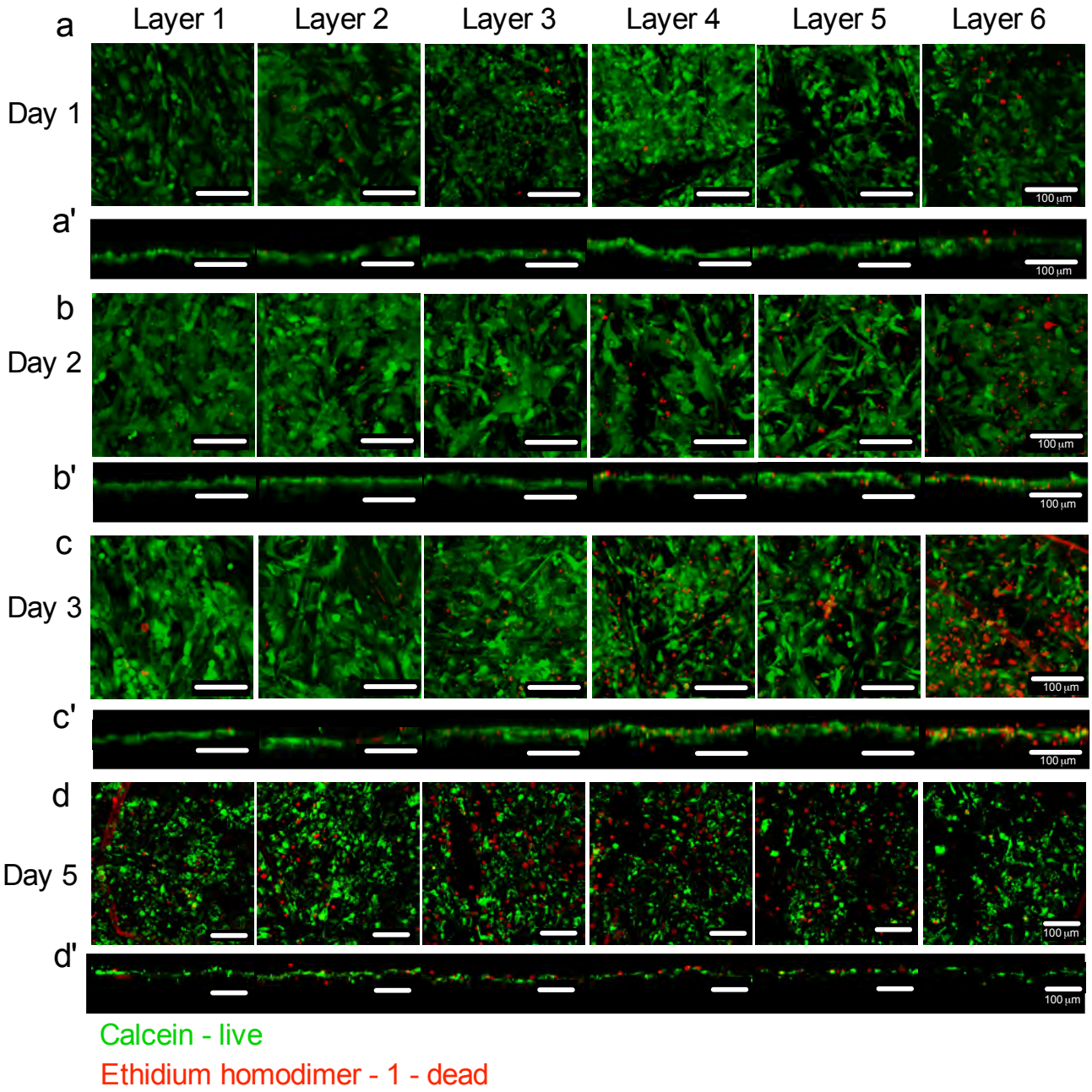

Supplementary Figure 9: Cell viability in each layer of the TRACER over time. a-d - Live cells (green) and dead cells (red) in each layer of the TRACER after (a) 1, (b) 2, (c) 3 and (d) 5 days of assembled culture. For each layer a top down projection and side profile are displayed (a'-d'). Note day 5 images show significantly less live cells.

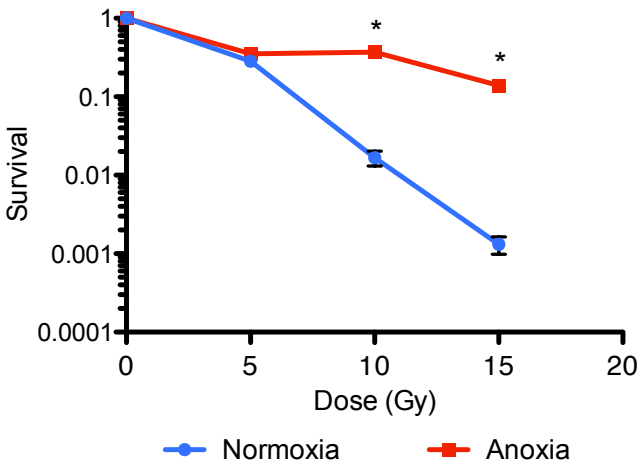

Supplementary Figure 10: Single layer normoxia and anoxia radiation dose controls. A single biocomposite layer maintained in either 21% pO2 (normoxia) or 0% pO2 (anoxia) was dosed with either 5, 10, or 15 Gy of radiation. Cell survival was assessed with a clonogenic assay. Data shows cells in anoxia are more resistant to radiation therapy when compared with those in normoxia. Data is normalized to a single layer cultured for 24h in normoxia and not treated with radiation. Error bars are SEM for n = 6 to 15 measurements from 1 or 2 samples. * indicates statistically significant differences with $p \leq 0.05$

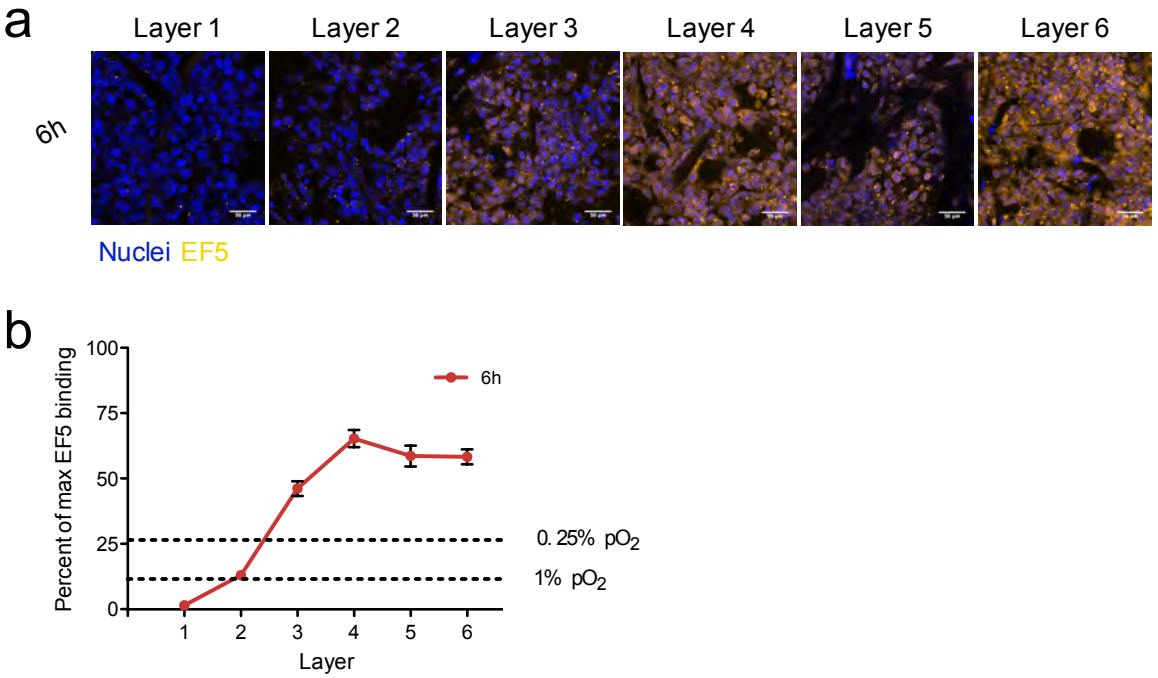

Supplementary Figure 11: Oxygen gradient measurements in TRACERs containing KP4 cells. a- EF5 staining in a TRACER containing KP4 cells and cultured in a rolled configuration for 6h. EF5 staining is shown in yellow and nuclei are shown in blue (DRAQ5). Images are 2um thick confocal optical sections. b- Nuclear EF5 staining intensity quantification of KP4 cells after 6h in the TRACER. Error bars are SEM for n = 18 measurements from 3 TRACERs.

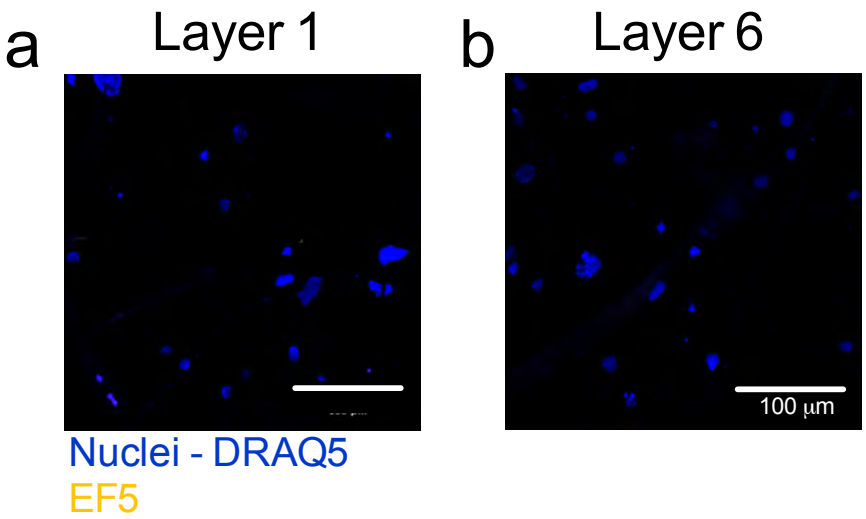

Supplementary figure 12: EF5 staining is absent in low cell density TRACERs. a-b- EF5 and nuclear staining in layers (a) 1 and (b) 6 of a low cell density (1x 107 cells/ mL collagen) TRACER after 24h of rolled culture. EF5 staining is shown in yellow and nuclear staining is shown in blue (DRAQ5) in each image. All scale bars are 100 microns. No EF5 staining is observed in either layer indicating no oxygen gradient is generated when low numbers of cells are present in the construct. This confirms that oxygen depletion to hypoxic levels in the inner layers of the TRACER occurs as a result of cellular consumption.

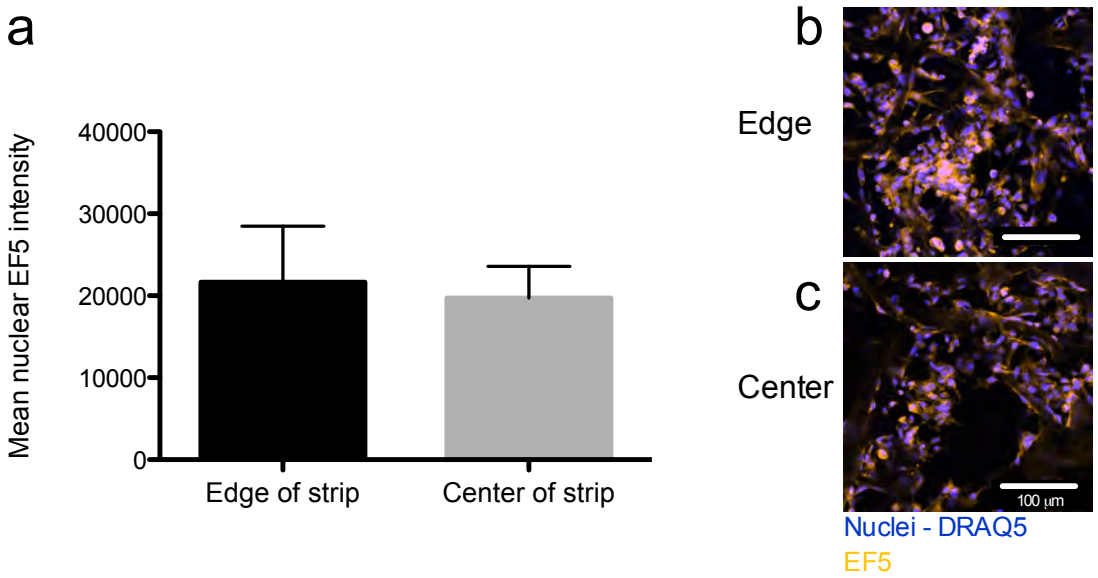

Supplementary figure 13: Oxygen levels at the edge versus centre of a layer. a- EF5 and nuclear staining in layer 6 of a TRACER (1 x 108 cells/mL collagen) after 12h of rolled culture at edge and centre locations (error bars are standard deviation from n = 6 images). Intensity at the edge versus centre of the strip was not statistically different (t-test, p = 0.56) b-c – Confocal images of EF5 staining at an edge (b) versus centre (c) location. EF5 staining is shown in yellow and nuclear staining is shown in blue (DRAQ5) in each image. No significant differences were observed in the levels of hypoxia in regions of a single layer located at the edge (proximal to the core) versus the centre of a layer. This suggests that oxygen levels were homogeneous between the edge and the centre regions of each layer.

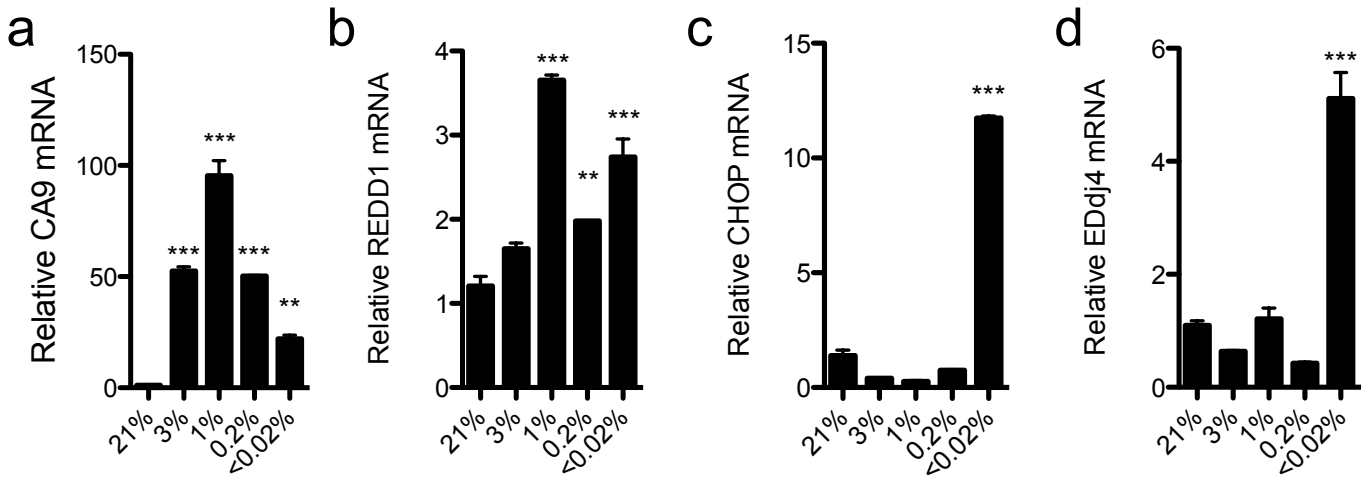

Supplementary Figure 14: SK-OV-3 cells hypoxia gene profile. Cells cultured in single layer non-rolled biocomposite sheets were exposed to normoxic (21%) and hypoxic (3%, 1%, 0.2%, <0.02%) conditions for 24h prior to analysis. mRNA of HIF1α target genes, CA9 (a) and REDD1 (b), and UPR target genes, CHOP (c) and ERdj9 (d), were quantified using qPCR, normalized to housekeeping gene RPL13a and relative to 21% control. Differences were assessed using One-way ANOVA, Dunnett post-test (* $p<0.05$, ** $p<0.01$, *** $p<0.001$). Error bars are SEM for n = 3 samples.

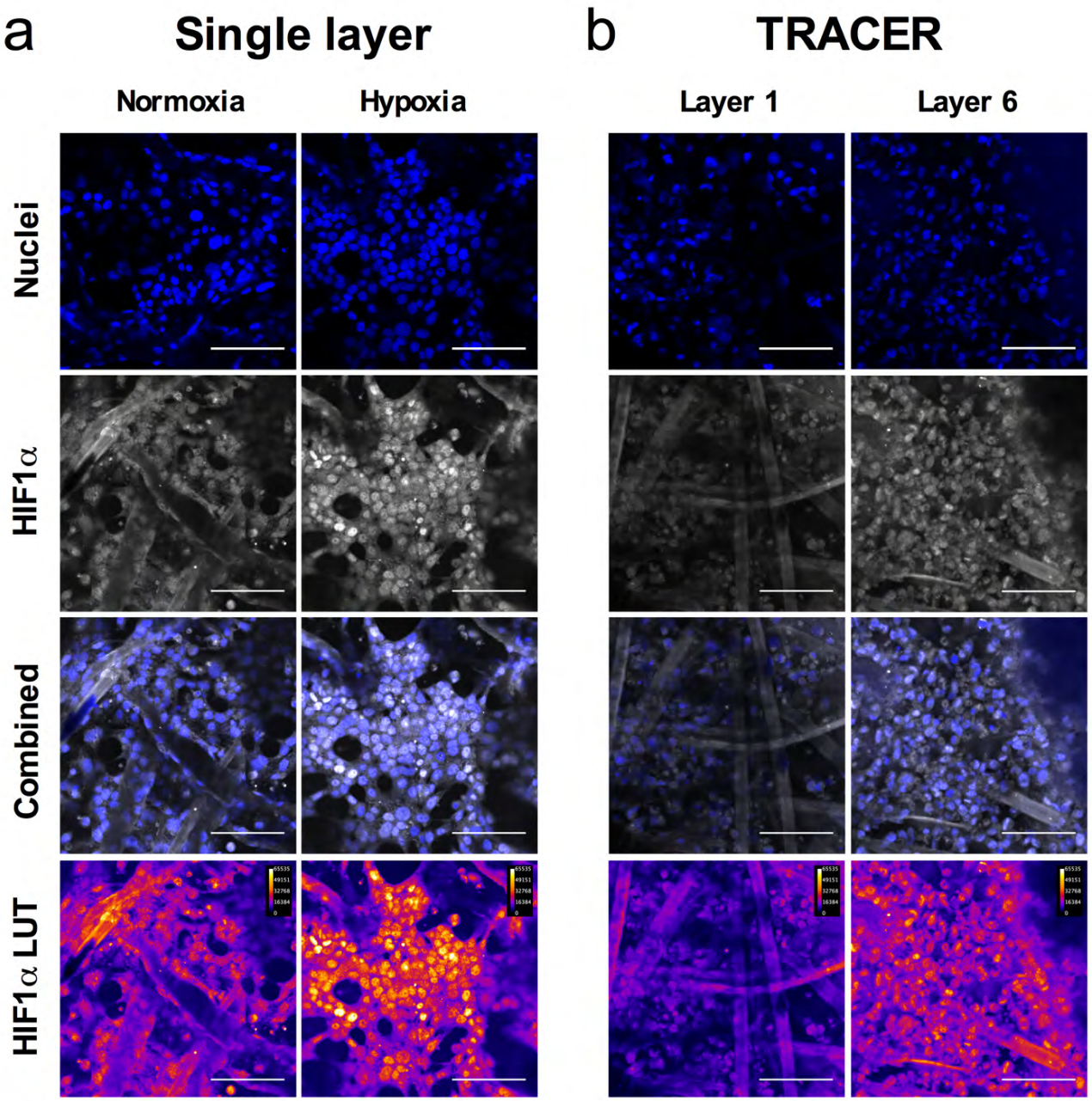

Supplementary Figure 15: Characterization of HIF1α localization in TRACER. a- Single biocomposite layers containing SK-OV-3 cells were cultured in normoxia (21% pO2), or exposed to hypoxia (0.2% pO2) for 4h prior to fixation and staining for HIF1α. In hypoxia, HIF1α is expected to translocate to the nucleus. Images are presented as nuclei (blue – DRAQ5), HIF1α (TRITC secondary, pseudo-colored white), and combined. To aid in visualization of HIF1α staining, the FIJI "Fire" LUT was applied to the HIF1α channel and is included (grayscale ramp provided at top right). b- Comparison panel images of layer 1 and layer 6 of a TRACER cultured for 4h prior to staining as described in (a). Images demonstrate an increase in HIF1α staining in the nuclear regions of the hypoxia control and layer 6 of the TRACER.

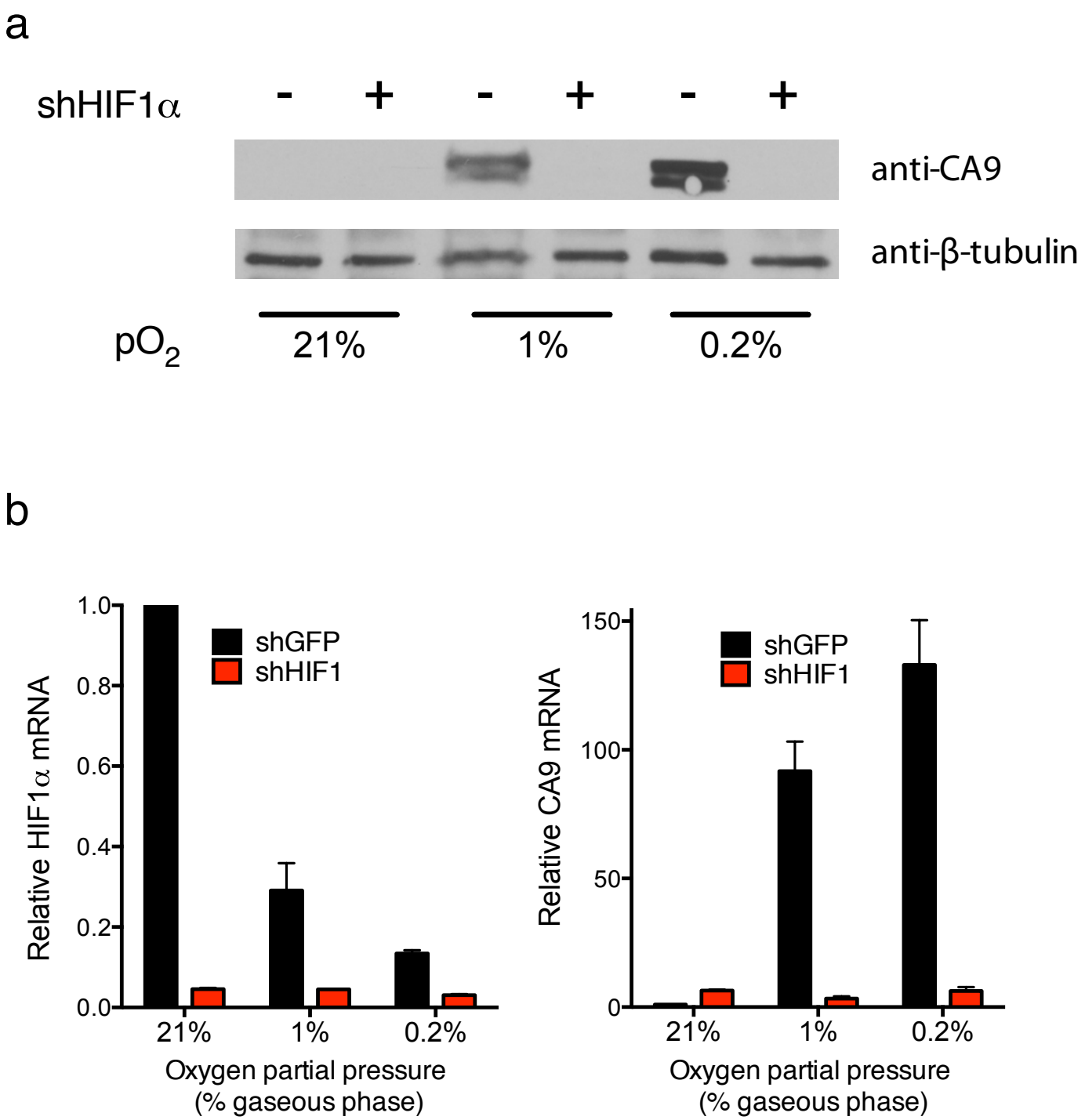

Supplementary Figure 16: Characterization of HIF knockdown cells SK-OV-3 cells stably expressing HIF1α shRNA or control shRNA were exposed to normal (21%) or hypoxic conditions (1% and 0.2%) for duration of 24h prior. a- western blotting was performed with an antibody against the HIF-induced gene, CA9, and anti-β-tubulin as control. b- The levels of HIF1α and CA9 mRNA relative to housekeeping gene RPL13a were quantified using quantitative reverse transcriptase–PCR analysis and normalized to the shGFP, 21% sample. Error bars are SEM with n = 3. HIF1α levels are significantly lower in shHIF versus shGFP (t-test with Bonferroni correction) at 21 and 0.2% oxygen. CA9 levels are significantly lower in shHIF versus shGFP (t-test with Bonferroni correction) under all conditions.

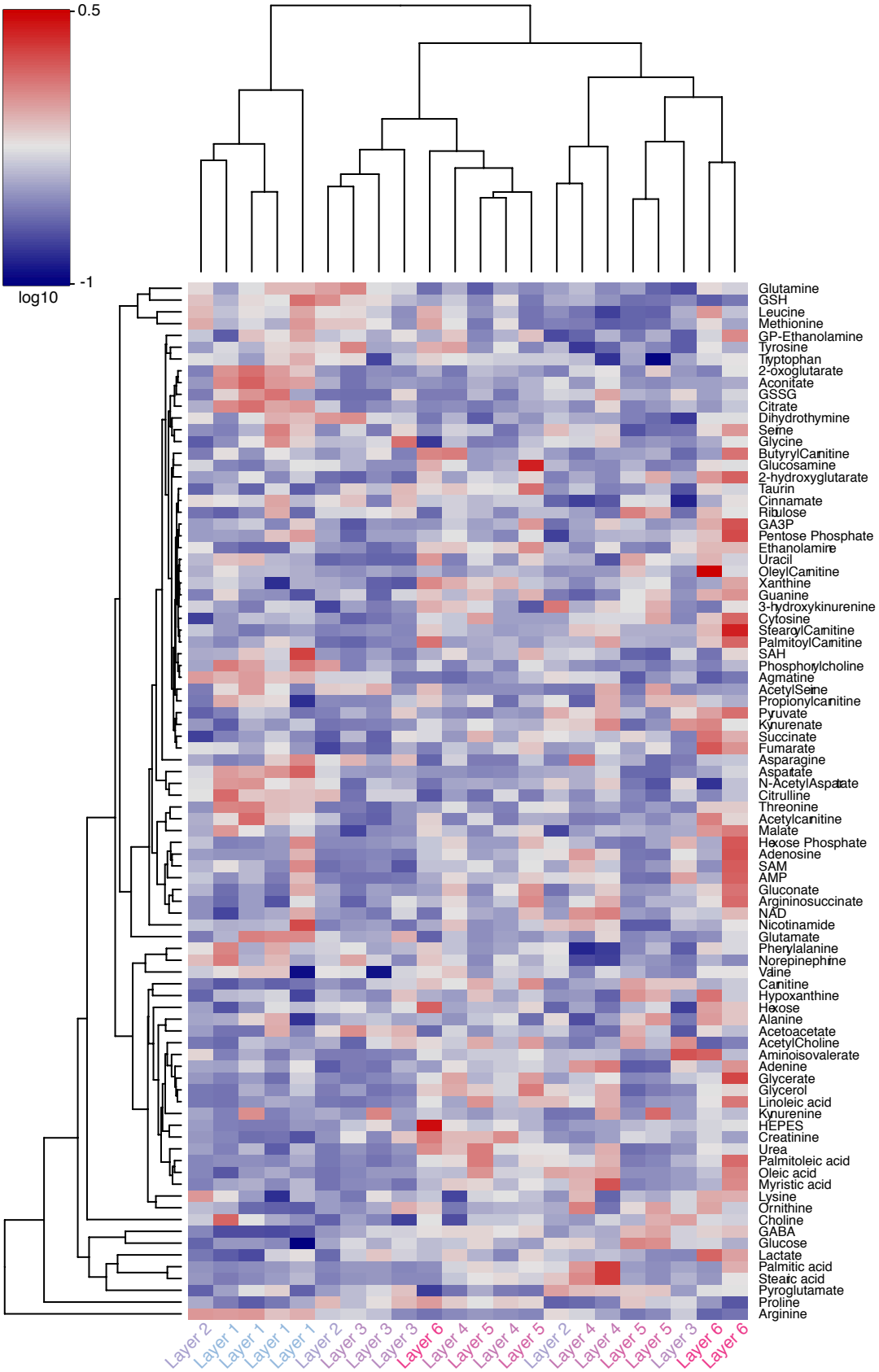

Supplementary Figure 17: Layer-specific unsupervised metabolomic analysis. Heatmap analysis of metabolites extracted from the indicated layers. Unsupervised hierarchical clustering of different layers (top dendrogram) and metabolites (left dendrogram) was performed. The log 10 of the relative abundance of each metabolite is color coded as indicated in the figure legend.

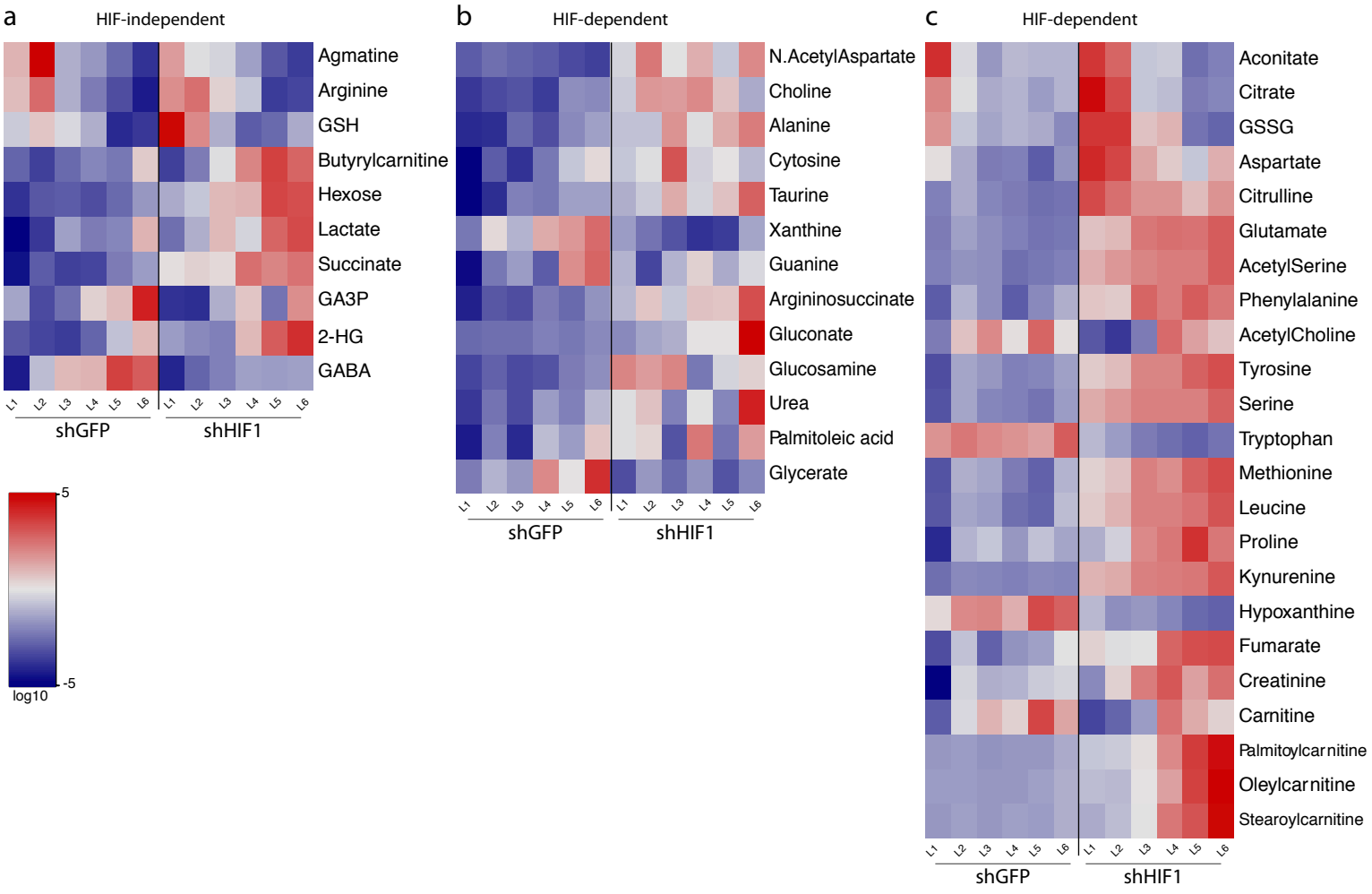

Supplementary Figure 18: Heatmap representation of metabolite intensities in each layer for metabolites that significantly correlate with hypoxia levels. Metabolite intensities per layer for metabolites showing significant correlation with hypoxia in both shGFP and shHIF conditions (a), or (b) in shGFP only, or (c) in shHIF only.

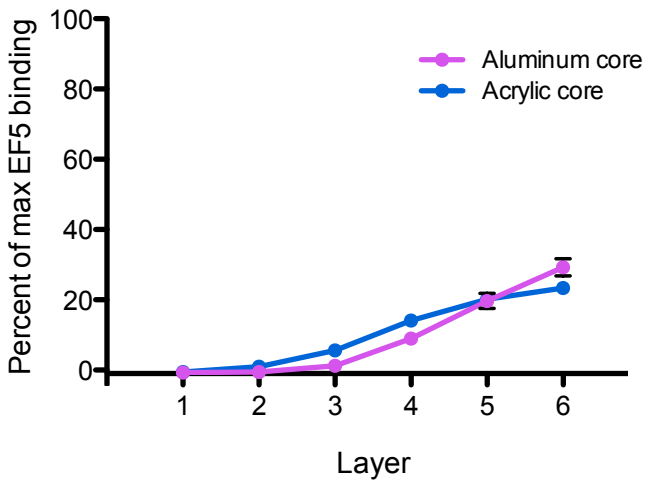

Supplementary Figure 19: Percent of EF5 binding on aluminum versus acrylic reactor cores. Acrylic as opposed to aluminum reactor cores were required for radiation experiments to reduce attenuation and ensure uniform irradiation of the cells. TRACERs assembled on acrylic versus aluminum cores showed similar EF5 binding gradients, confirming oxygen could not significantly diffuse though the acrylic core. Error bars are SEM for n = 18 measurements from 3 aluminium core TRACERs, and n = 12 measurements from 2 acrylic core TRACERs.

Supplementary Table 1: Summary table showing fold change in metabolite level between shGFP versus shHIF in layer 1 samples

Metabolite	Fold Change	p-value	Benjamin-Hochberg significant p- value
Palmitoyl_Carnitine*	5.0338	0.0002	0.0006
Oleyl_Carnitine*	4.4996	0.0002	0.0011
Stearoyl_Carnitine	4.4135	0.0437	0.0163
Glucosamine*	4.2002	0.0004	0.0017
Kynurenine*	3.0236	0.0042	0.0062
Palmitoleic_Acid	2.8536	0.3362	0.0348
HEPES	2.4895	0.1475	0.0281
Urea	2.4512	0.1400	0.0264
Citrulline	2.3271	0.0312	0.0140
O.AcetylSerine*	2.1904	0.0033	0.0045
Succinate	2.0989	0.0570	0.0191
Amino.isovalerate	2.0859	0.2954	0.0337
Glucose	2.0479	0.0415	0.0157
Argininosuccinate	1.9513	0.0367	0.0152
Linoleic_Acid	1.9354	0.2086	0.0320
AMP	1.8304	0.3747	0.0365
Malate*	1.8083	0.0013	0.0028
Oleic_Acid	1.8011	0.1626	0.0292
Gluconate	1.7660	0.1148	0.0242
Hexose	1.7094	0.0651	0.0208
Ethanolamine	1.6347	0.0209	0.0112
Valine	1.5851	0.0344	0.0146
Serine*	1.5769	0.0037	0.0051
Glycine*	1.5416	0.0012	0.0022
Kynurenic_acid_pos	1.5414	0.3237	0.0343
Citrate	1.5310	0.0525	0.0180
Acetoacetate	1.5149	0.1458	0.0275
Pyroglutamic_Acid	1.5078	0.0106	0.0096
Taurin	1.4849	0.0118	0.0101
Fumarate*	1.4818	0.0019	0.0034
GSH	1.4808	0.1232	0.0253
Lysine	1.4512	0.0561	0.0185
N.AcetylAspartate	1.4450	0.0736	0.0219
Ribulose	1.4390	0.1357	0.0258
Tyrosine*	1.4235	0.0056	0.0079
Glycerol	1.4231	0.4696	0.0382
Norepinephrine	1.4194	0.0614	0.0202
Alanine	1.4181	0.0660	0.0213
Aspartate*	1.4180	0.0051	0.0073
Creatinine	1.3910	0.0219	0.0118
Myristic_Acid	1.3861	0.5926	0.0410
Leucine	1.3837	0.0266	0.0135
Glutamate*	1.3797	0.0020	0.0039

Methionine	1.3773	0.0489	0.0169
Phenylalanine	1.3764	0.0099	0.0090
Ornithine	1.3758	0.0504	0.0174
Palmitic_Acid	1.3742	0.6308	0.0421
X3.hydroxykinurenine	1.3682	0.0232	0.0129
HexosePhosphate	1.3631	0.6874	0.0438
X2.HG	1.3594	0.1680	0.0303
Glutamine	1.3565	0.1445	0.0270
Dihydrothymine	1.3564	0.1501	0.0287
Asparagine	1.3380	0.0914	0.0230
Cytosine*	1.3340	0.0045	0.0067
Phosphorylcholine	1.3321	0.2571	0.0326
Threonine*	1.3288	0.0037	0.0056
GSSG	1.3247	0.6495	0.0433
Choline	1.3104	0.0584	0.0197
Guanine	1.2966	0.1139	0.0236
Proline	1.2779	0.0228	0.0124
Cinnamate	1.2679	0.1653	0.0298
Lactate	1.2613	0.1824	0.0315
Stearic_Acid	1.1939	0.7538	0.0472
NAD	1.1680	0.5691	0.0399
S.Adenosyl.Methionine	1.1378	0.7222	0.0461
GABA	1.1362	0.2878	0.0331
Adenine	1.1250	0.6928	0.0444
S.Adenosyl.Homocysteine	1.1220	0.5640	0.0393
Arginine	1.1114	0.5954	0.0416
Pyruvate	1.0942	0.6930	0.0449
Nicotinamide	1.0862	0.7366	0.0466
Xanthine	1.0760	0.4601	0.0376
Agmatine	1.0729	0.7994	0.0478
Adenosine	1.0611	0.8853	0.0489
Uracil	1.0282	0.8054	0.0483
Propionylcarnitine	0.9737	0.9435	0.0500
Aconitate	0.9699	0.7217	0.0455
AcetylCholine	0.9342	0.6437	0.0427
Pentose_Phosphate	0.9304	0.9072	0.0494
Carnitine	0.9200	0.5089	0.0388
aKG	0.8729	0.3629	0.0360
ButyrylCarnitine	0.8513	0.5881	0.0404
Hypoxanthine	0.8340	0.1199	0.0247
Glycerylphosphorylethanolamine	0.8242	0.0829	0.0225
Acetylcarnitine	0.8130	0.1721	0.0309
Glyceraldehyde_3.phosphate	0.6841	0.4183	0.0371
Glycerate	0.6678	0.3585	0.0354
Glycerylphosphorylcholine*	0.6609	0.0073	0.0084
Tryptophan	0.4775	0.0192	0.0107

Supplementary Table 2: Comparison of cell numbers required for TRACERs with different geometries

w (cm)	d (cm)	t (cm)	cell density/ml	cells/layer	total # cells*
1	0.6	0.004	100,000,000	753,982	4,523,893
0.5	0.6	0.004	100,000,000	376,991	2,261,947
0.1	0.6	0.004	100,000,000	75,398	452,389
1	0.1	0.004	10,000,000	12,566	75,398
0.5	0.1	0.004	10,000,000	6,283	37,699
0.1	0.1	0.004	10,000,000	1,257	7,540

*Assuming 6 layer TRACER

w biocomposite strip width

d core diameter

t construct thickness

highlighted line indicates current TRACER design

Supplementary Table 3: Details of antibodies used

Antibody	Figure in Paper	Supplier	Catalogue Number	Clone Number	Reference
Anti-EF5-Cy3 (ELK3-51)	3a,b,c,h SI 11a,b SI 12a,b SI 13a,b,c SI 19	University of Pennsylvania (Hypoxia-Imaging.org)			Koch CJ. Measurement of absolute oxygen levels in cells and tissues using oxygen sensors and 2-nitroimidazole EF5. Methods in Enzymology. 352:3-31, 2002.
Anti-Ki-67	SI 2f	Merck Millipore	AB9260		
Anti-ZO1	SI 7a,b,c,d	InVitrogen	339100		
Anti-HIF1α	SI 15a,b	GeneTex	GTX61608		
Anti-CA9	SI 16a	Gift from Dr. Silvia Pastorekova		M75	Pastorekova S, Zavadova Z, Kostal M, Babusikova O and Zavada J (1992) A novel quasi-viral agent, MaTu, is a two-component system. Virology 187: 620–626
Anti-β-tubulin	SI 16a	Abcam	ab6046		
Secondary Goat Anti-Rabbit TRITC	SI 13a,b	Sigma	T-6778		
Secondary Goat Anti-Mouse 488	SI 7a,b,c,d	Life Technologies	A11029		
Secondary Goat Anti-Rabbit 488	SI 2f	ThermoFisher Scientific	A-11008		

Supplementary Table 4: Details of statistics

Figure	Device n	Technical Replicate per Layer	n used in statistics/ error bars	Statistics Performed	Test Assumptions	Justification of Test Choice
2A	3	3	3	ANOVA Bonferroni or Games-Howell	normality and equal (Bonferroni) or unequal (Games-Howell) variance	Levene's test for homogeneity used to test equal variance; QQ plot used to test normality
2B	3	3	3	Bonferroni or Games-Howell post-test	normality and equal (Bonferroni) or unequal (Games-Howell) variance	Levene's test for homogeneity used to test equal variance; QQ plot used to test normality
2C	3	1	3	ANOVA Games-Howell post-test	normality and unequal variance	Levene's test for homogeneity used to test equal variance; QQ plot used to test normality
2D	6h: 3, 24h: 4	6	6h: 3, 24h: 4	N/A		
2E	2	9 (1 or 2 dilutions in triplicate)	9	T test with Bonferroni correction	normality and equal variance	F test used to test equal variance; QQ plot used to test normality
3B	3	6	3	N/A		
3C	3	6	3	N/A		
3D	3	1	3	ANOVA Dunnett post-test	normality and equal variance	Test for comparing multiple groups to a control group (layer 1). Normality confirmed by QQ plots.
3E	3	1	3	ANOVA Dunnett post-test	normality and equal variance	Test for comparing multiple groups to a control group (layer 1). Normality confirmed by QQ plots.
3F	3	1	3	ANOVA Dunnett post-test	normality and equal variance	Test for comparing multiple groups to a control group (layer 1). Normality confirmed by QQ plots.
3G	3	1	3	ANOVA Dunnett post-test	normality and equal variance	Test for comparing multiple groups to a control group (layer 1). Normality confirmed by QQ plots.
3H	3	6	3	ANOVA Bonferroni or Games-Howell	normality and unequal variance	Test for comparing multiple groups to a control group (layer 1). Normality confirmed by QQ plots.

4	4	1	4	Pearson or Spearmann Correlation	normality and collinearity	Shapiro Wilk's test and Ramsey Regression Equation Specification Error Test (RESET)
SI 2E	3	3	3	ANOVA Bonferroni or Games-Howell post-test	normality and equal (Bonferroni) or unequal (Games-Howell) variance	Levene's test for homogeneity used to test equal variance; QQ plot used to test normality
SI 2F	3	3	3	ANOVA Bonferroni or Games-Howell post-test	normality and equal (Bonferroni) or unequal (Games-Howell) variance	Levene's test for homogeneity used to test equal variance; QQ plot used to test normality
SI 3	1	3	3	N/A		
SI 5A	1	12	12	ANOVA Bonferroni or Games-Howell post-test	normality and equal (Bonferroni) or unequal (Games-Howell) variance	Levene's test for homogeneity used to test equal variance; QQ plot used to test normality
SI 5B	1	12	12	N/A		
SI 10	1 or 2	1 to 5	6 to 15	T test with Bonferroni correction	Normality and un-equal variance	F test used to test equal variance; QQ plot used to test normality
SI 11b	3	6	18	N/A		
SI 13a	1	6	6	pooled T-test	normality and equal variance	F test used to test equal variance; QQ plot used to test normality
SI 14	3	1	3	ANOVA Dunnett post-test	normality and equal variance	Test for comparing multiple groups to a control group (layer 1). Normality confirmed by QQ plots
SI 16b	3	1	3	T test with Bonferroni correction	normality and equal (pooled test) or unequal variance (unpooled test)	F test used to test equal variance; QQ plot used to test normality
SI 17	4	1	4	N/A		
SI 18	4	1	4	Pearson or Spearmann Correlation	normality and collinearity	Shapiro Wilk's test and Ramsey Regression Equation Specification Error Test (RESET)
SI 19	Al 3, Ac 2	6	Al: n=18, Ac: n=12	N/A		